RESEARCH ARTICLE

ISSN: 2455-8095
doi: 10.21477/ijapsr.4.2.2

Removal of Chrysoidine Y from water by Graphene-based Nanocomposite Derivatives with Magnetic Chitosa Nanocomposite

Farid Abu Shammala[1]*, Barry Chiswell[2]

[1]Adjunct Professor, Department of Pharmacy, University of Palestine , El-Zahra City, Gaza, Palestine
[2]National Research Centre for Environmental Toxocology, University of Queensland , Brisbane, Australia.

ABSTRACT

This article describes a novel and efficient MCTS/GO nanocomposite for the accumulation and removal of a hazardous azo dye (Chrysoidine Y) from its aqueous solutions. Magnetic Chitosan /graphene oxide (MCTS/GO) nanocomposite adsorbent was prepared by wet-spinning technique, was used as accumulation and removal of Chrysoidine Y from aqueous solution. The structure and morphology of MCTS/GO nanocomposites were investigated using transmission electron microscope (TEM) and Fourier transform infrared (FTIR) spectroscopy were carried out on the MCTS/GO before the Chrysoidine Y (CY) accumulation experiments. The adsorption kinetics and isotherm studies were conducted under different conditions (pH = 3-7 and CY concentration = 100-400 mg/L) to examine the accumultion efficiency of the MCTS/GO towards CY in aqueous solution. The kinetics data of the adsorption process were analyzed using different kinetic models in order to investigate the adsorption behavior of CY on MCTS/GO. The results showed that the maximum adsorption capacity of the MCTS/GO nanocomposites towards CY can achieve up to ~700 mg/g for the adsorption at 300 mg/L CY. Kinetic data of adsorption process were found to fit pseudo-second order model as compared with pseudo-first-order model. The intraparticle diffusion model suggested that the adsorption process of MCTS/GO towards CY was dominated by the external mass transfer of CY molecules to the surface of MCTS/GO.

Keywords: magnetic chitosan, graphene oxide, fibres, adsorption, chrysoidine Y, desorption

1. INTRODUCTION

Nowadays, toxic chemical compounds have become the main cause of water pollution. Water pollution exerts negative impacts not only on species living in the water but also on the broader biological community in our environment. Recently for instance, organic dyes are often discharged through wastewater into the local environment without adequate treatment. Dyeing chemicals are extensively used for some food industries, treatment of cosmetics, textiles, leather articles, plastics, printing and paper industries, and can end up in wastewaters and are therefore a potential source of pollution of lakes, rivers and waterways (Brindley, 2009). Moreover, azo dyes serve as key components in high-tech applications such as optical data storage, light-emitting diodes, and laser welding processes, display devices, reprographics, dye-sensitized solar cells, energy transfer cascades, light – emitting diodes; laser welding processes, or heat management systems. The presence of these dyes in wastewater is a gaining growing concern due to their potential health hazards and environmental pollution. Because of the complex aromatic structures and xenobiotic properties of dyes, they are not easy biodegradable and harmful to human beings (Parida et al., 2001). The azo dyes are organic compounds bearing the functional group R–N=N–R′, in which R and R′ are usually aryl. They are a commercially important family of azo compounds, i.e. compounds containing the linkage C-N=N-C are chemically related to azo dyes are azo pigments, which are insoluble in water and other polar solvents (Mittal et al., 2010; Meral and Metin, 2014). In many countries, there is a ban on the import, sale and use of a specific blue azo pigment, and azo pigments that may release carcinogens, as well as certain products containing azo pigments. The regulations exist in order to limit the use of azo pigments that are harmful to health and the environment. Indeed, certain azo pigments may form

Corresponding author
Farid Abu Shammala
Email: drfaridshammala@hotmail.com

Received: 12-12-2018 **Accepted:** 10-02-2019 **Available Online:** 01-04-2019

carcinogenic substances (arylamines) or are toxic to the aquatic environment, and disposal of these dyes into water bodies leads to tremendous environmental pollution (Mittal et al., 2010).

Because of simplicity, several kinds of methods have been used for accumulation and removal of dyes from wastewater, such as extraction, photocatalytic degradation, ion exchange, membrane filtration, biological treatment and adsorption (Meral and Metin, 2014; Aksu, 2005; Santos and Boaventura, 2008; Li et al., 2011; Coasne, 2011; Du, 2014; Sadrnourmohamadi and Gorczyca, 2015; Kumar et al., 2015). Based on simplicity, ease of operation and high efficiency, adsorption is deemed as a high-efficient and economical technology for dye removal. Among the most used methods, adsorption was proved an effective method due to its low cost, high efficiency, and simple operation. In order to meet the increasingly effluent discharge standards and resolve the stringent problem of dye pollution, the scientists have been searching for environmentally friendly, highly efficient, and low cost adsorbents. In addition, adsorption combined with magnetic separation technology has gained much attention in recent years and extensively used technique for dye sequestration due to its easy phase separation from aqueous environmental solution and its capability of treating a mass of wastewater in few minutes (Aksu, 2005). For instance, magnetic separation of toxic pollutant is becoming a potential method in wastewater treatment and purification, and found to have predominant significance in the removal of toxic dyes more effectively compared to conventional method of treatments. Indeed, numerous natural and synthetic adsorbents were used, out of which magnetic composites (MCs) and magnetic nanocomposites (MNCs) have received much attention presently in the removal of toxic dyes from aqueous solution (Santos and Boaventura, 2008; Li, 2011; Coasne et al., 2011; Du et al., 2014; Du, 2015; Kumar et al., 2015; Kar et al., 2009; Gulshan et al., 2010; El-Naas et al., 2009; Yao et al., 2010).

However, with the rapid development in nanotechnology techniques, carbon nanomaterials have been studied for water treatment, such as the carbon nanotubes (Liu et al., 2012). Graphene's oxidised derivative, graphene oxide (GO), also possesses some outstanding removal properties including good mechanical strength, abundant oxygen-containing and, therefore, hydrophilic functional groups, and large surface area. Furthermore, GO can be easily produced in bulk via a chemical exfoliation process of natural graphite (Liang, 2009; Su et al., 2009; Park and Ruoff, 2009; Dreyer et al., 2010; Yang et al., 2011; Wang et al., 2013; Wu et al., 2014). Due to graphine advantages, GO has proven to be a promising adsorbent for removal of dye pollutants from water. There are many publications, which report that the synthetic GO can be used directly for water treatment and exhibit high adsorption capacities toward dyes (Tao, 2014; Du et al., 2014; Li et al., 2013; Shi et al., 2014; Pati et al., 2015).

Indeed, graphene-based polymer nanocomposites exhibit superior promising properties. For example, graphene-based polymer composites showed better thermal, electrical and mechanical properties than the normal polymer (Li et al., 2015). It was shown that the mechanical and electrical properties of graphene-based polymer composites are much better in comparison to clay or other carbon filler-based polymer composites (Layek et al., 2012; Jagiello et al., 2014; Krishnan et al., 2012; Singh et al., 2011; Malafaya et al., 2007). One of the main applications of graphene sheets is its wide use as reinforcement agents for the preparation of nanocomposites with different types of polymers. Beside the mechanical properties, electrical and thermal properties of the polymeric matrix can also be enhanced. It is a fact that the graphene-based nanocomposites showed improved properties compared to the original raw form of graphene. For example, graphene nanocomposites with polysaccharides such as chitosan have gained many diverse new applications. Polysaccharide exist both as linear or branched polymers, since their repeating monosaccharide units are connected via O-glycosidic bonds (Shelke et al., 2014). Their properties include water solubility, gelation and other surface properties that depend on the type of the monosaccharide composition being applied. Advantages such as abundance in nature, biocompatibility, biodegradability, easy functionalization and relatively easy isolation from their natural sources have led to their study and use for several applications, especially in the field of drug delivery and biomaterials (Kyzas et al., 2014). Another application gained by graphene derivatives with polysaccharide is the use in accumulation and removal of various types of pollutants from wastewater effluents (Travlou et al., 2013). Previous research has shown that graphene nanocomposites with chitosan have been used for the removal of dyes (Travlou et al., 2013; Kyzas et al., 2014), heavy metal ions (Parida, KM et al., 2011) and pharmaceutical compounds (Kyzas et al., 2014) from aqueous solutions. Despite the intriguing properties of polysaccharides, their poor mechanical properties limit their applications in this field. Nanofillers such as graphene are known to improve the properties of raw polymers, not only the mechanical but also the thermal and electrical properties (Du and Cheng, 2012; Das and Prusty, 2013). Moreover, the effectiveness of the incorporation of both graphene and graphene oxide together in raw polymers have been extensively studied, mostly synthetic polymers

reinforced by graphene and graphene oxide find several improvement in properties such as mechanical strength, thermal stability, gas barrier properties, electrical and thermal conductivity etc. (Sun et al., 2013; Kim et al., 2010; Huang et al., 2012; Zhang et al., 2014; Tjong, 2014; Kuang, 2013; Kuang and Hu, 2013; Rinaudo, 2008; Draget, 1997).

In this research article, we prepared from graphite oxide (GO) and magnetic chitosan (MCTS) a nanocomposite material (MCTS/GO) and used it to investigated its capability for accumulation and removal of Chrysoidine Y from wastewater. Chitosan (CTS) with molecular weight (Mw) ˜810 kDa and degree of deacetylation (DDA) ˜83% was synthesized in our laboratory from prawns shell. And graphene oxide (GO) was prepared by improved Hummers method. The MCTS/GO nanocomposites were synthesized by adding magnetic Fe3O4 particles into the CTS/GO nanocomposite fibers, followed by the dispersion of GO in the magnetic CTS solution via ultrasonication. The graphine-based nanocomposite derivative with magnetic chitosan were applied in the accumulation and removal of Chrysoidine Y under visible and UV light. CTS/GO nanocomposites were lyophilized using formic aldehyde as a cross-linked to obtain the hydrogels. These will be compared regarding their mechanical properties as well as their various applications. The effect of GO on the properties of chitosan films has been studied using solution mixing. Also, the strong interactions between the functional groups of the two components tested, confirmed by FTIR spectra, led to a series of improved properties, including mechanical strength in both wet and dry state, storage modulus, and thermal stability. Indeed, the fabricated CTS/GO nanocomposite material which was synthesized from chitosan (CTS) with graphite oxide (GO) have large surface area, better mechanical and thermal properties and high adsorption capacity for Chrysoidine Y than either CTS or GO alone.

2. MATERIALS AND METHODS

2.1. Materials

Graphene (GE), Chrysoidine Y and magnetic chitosan (MCTS) used in our studies were purchased from Sigma-Aldrich. Analytical grade chemical reagents like potassium persulfate ($K_2S_2O_8$) and hydrochloric, sulfuric, and nitric acid used in our experiments were obtained from Sigma Chemicals. GE was reacted with mixture of two acids H_2SO_4 and HNO_3 acids with 3 : 1 ratio and later sonicated for 60 minutes using an ultrasonic sonicator to form carboxylic acid functionalized GO (GO-COOH). The conversion of carboxylic acid group to formyl chloride was done by reaction with thionyl chloride for 24 h at 80°C. Then the reaction was stopped, and the mixture was cooled before centrifuging and washing to remove excess reactants. The sample was then dried overnight at a temperature of 90°C and 30 Hg pressure.

2.2. Synthesis of GO-magnetic Chitosan

The formyl chloride of GO (GO-COCl) (400 mg) was then reacted with chitosan (2 g) in 100 mL 2% acetic acid at 75°C for 24 hours while magnetic stirring. In order to remove the unreacted chitosan, the product was washed three times with 3% acetic acid after the reaction was stopped.

2.3. Synthesis of GO-magnetic Chitosan Grafted Derivative

Chitosan complex (0.1 g) was then reacted with $K_2S_2O_8$ (0.02 g) in 2% acetic acid solution at 80°C for 4 h to form the nanocomposite product MCTS/GO. The final product was prepared by centrifuging at 20,000 rpm and washing the sample three times with deionized water before drying at 90°C. The MCTS/GO was produced using a chemical co-precipitation method with iron oxide. Iron (III) oxide (Fe2O3) nanoparticles (5.8 g) were produced by dissolving ferrous ammonium sulfate in (10.7 g) of ammonium ferric sulfate in 100 mL deionized water to form a mixed iron salt solution under oxygen-free conditions. Chemical precipitation was achieved by adding a 75 mL ammonium hydroxide (NH4OH) solution (30.0%) drop-wise for a period of 30 min at 30°C. After the addition of ammonium hydroxide a black precipitates appeared immediately and the precipitated particles exhibited a strong magnetic response. Next, 2 g dry MCTS/GO was dispersed in 200 mL ultrapure water using ultra-sonication to form a stable suspension. Finally, the MCTS/GO solid was collected using a magnet and was washed with deionized water and anhydrous ethanol three times each and dried at 90°C for 24 h in a vacuum oven. Our results shows a strong affinity between water and the different groups attached to graphene sheets. Indeed, dispersions with water show the darkest colour for the longer time, pure graphite can be dispersed only partially and a high number of particles remain adhered to the container walls. However, after sonication and 12 h kept at rest the carboxyl and hydroxyl groups in GO and MCTS allows the formation of a stable dispersion in water. For chitosan-grafted samples, the hydrophilic nature of chitosan facilitates the interactions between both water and amine, as well as hydroxyl and carbonyl groups. However, it is important to mention that dispersion related to graphene oxide grafted with chitosan obtained at the temperature range of 60°C is better after 24 h than the other samples of grafted graphene oxide. On the other hand, we observed that the dispersion of graphene oxide in hexane is poor, the absence of suitable chemical groups

to interact and the non-polar nature of the solvent cause the nanosheets to precipitate rapidly, regardless of moieties attached to MCTS/GO and grafted samples.

2.4. Adsorption Procedure

The prepared MCTS/GO nancomposites with superparamagnetism were then used to test adsorption ability for dye. The prepared MCTS/GO nancomposites with superparamagnetism can be separated by a magnet after the adsorption process. All sorption experiments were performed in triplicate and the average values were adopted. The maximum deviation for the duplicates was usually less than 5%; 5 mg absorbents and 50 ml dye solution were put in 50 ml glass bottles and processed within an incubator shaker at a frequency of 100 r.p.m. The initial concentration of dye is 0–50 mg L–1. Meanwhile, the blank experiments without absorbents were also conducted to confirm that the decrease of dye concentration was because of absorbents instead of any other factors. After the adsorption process, the dye concentration was measured by the UV spectrophotometer at the peak of λmax. A calibration curve between absorbance and concentration of dye (0 - 20 mg L–1) was constructed according to the Beer–Lambert's Law. For solutions with concentration higher than 20 mg L–1, the solutions were first diluted with deionized water. Kinetic studies were performed at a constant temperature of 25°C and 100 r.p.m. with 50 mg L–1 initial concentration of dye solutions with different adsorption time. The solid–liquid ratio experiments were conducted in 100 mg L–1dye solutions with varying solid–liquid ratio from 1:10 to 1:2. The effect of dye solution pH on the accumulation and removal of drug was studied in the range of 3–10 with 100 mg L–1initial concentrations of dye solutions. The initial pH values of all the solutions were adjusted using 0.1 mol L–1 HCl or 0.1 mol L–1 NaOH solution with desired concentrations. The ionic strength experiments were conducted in 100 mg L–1 dye solutions with varying ionic strength range from 0 to 2. 5 mmol L–1.

3. RESULTS AND DISCUSSION

3.1. Characterization Using SEM and TEM Image

Figure 1 shows the Scanning Electron Microscopy (SEM) images of (a) GO and (b) Chitosan (c) MCTS/GO before adsorption and (d) MCTS/GO after adsorption. It is obvious in Figure 1 the sheet-like structure, corrugated morphology exists, indicating the characteristics of single-layers of GO and MCTS/GO sheets. The results revealed small number of magnetite nanoparticles with an average size of 10 nm, uniformly decorate the surface of GO sheets. Figure 1A shows a typical 2D flake-like morphology of GO sheets. Figure 1b reveals the porous nanostructures of lyophilized MCTS/GO nanocomposites, suggesting that the GO sheets were cross-linked in the porous CTS networks. The images show GO is dispersed in the composite due to the formation of agglomerates at length scales of tens of microns. The typical SEM image of GO presents a wrinkled sheet-like structure, as shown in Figure 1A. Figures 1C shows a better distribution of GO particles homogeneously covered by the Chm polymer. The results showed copolymer-modified graphene composite can be homogeneously integrated within hydrophilic Chm matrix. The presence of ionic moieties such as alkyl amino- and carboxylates in the polymer backbone can result in enhanced interfacial interactions between the filler and the matrix. Upon functionalization with MCTS/GO, the SEM image of MCTS/GO (Figure 1C) has greater thickness and a much rougher surface, which demonstrates that many polymer chains have been assembled on the surface of the GO sheets. Figure 2 shows the Transmission Electron Microscopy (TEM) image of (a) GO, the (b) CTS/GO before adsorption and the (c) MCTS/GO after adsorption. As shown in Figure 2A GO transparent sheet like structure with the presence of folded regions at the edges. TEM image of the MCTS/GO (Figure 2C and Figure 2D) presents a thick and rough sheet-like material, demonstrating that MCTS composites have been assembled on the GO sheets. Indeed, there are small magnetic nanoparticles with an average size of 10 nm, uniformly decorate on the surface of GO sheets. These results prove effectively that Fe_3O_4 nanoparticles are successfully modified on the surface of GO sheets.

3.2. Characterization Using X-ray diffraction patterns

In addition, the strong interaction between CTS and GO was also evidenced by X-ray diffraction studies. The XRD patterns of graphite and graphene oxide are depicted in Figure 3a, b performed in the range of 5o-70o. The diffraction angles of the graphite peak 26.6025o with d-spacing 3.34810 Å. The results revealed that graphene oxide form a new peak at 9.0715o with d-spacing 9.74063Å. The change of angle XRD patterns are shifted towards the left shows the occurrence of a material change to the nature and crystallinity of graphine oxide, and that it was reduced. In fact, the shown widening of distances between the layers of graphite of 3.34810 Å into Graphene oxide at 9.74063 Å occurs due to the formation phenol group, ketone group, epoxy group, carboxyl group, and a carbonyl group. The addition of H molecules, O2 and clusters of oxygen also causes graphene oxide to have a wider d-spacing. Figure 3c shows the diffraction patterns for the lyophilized

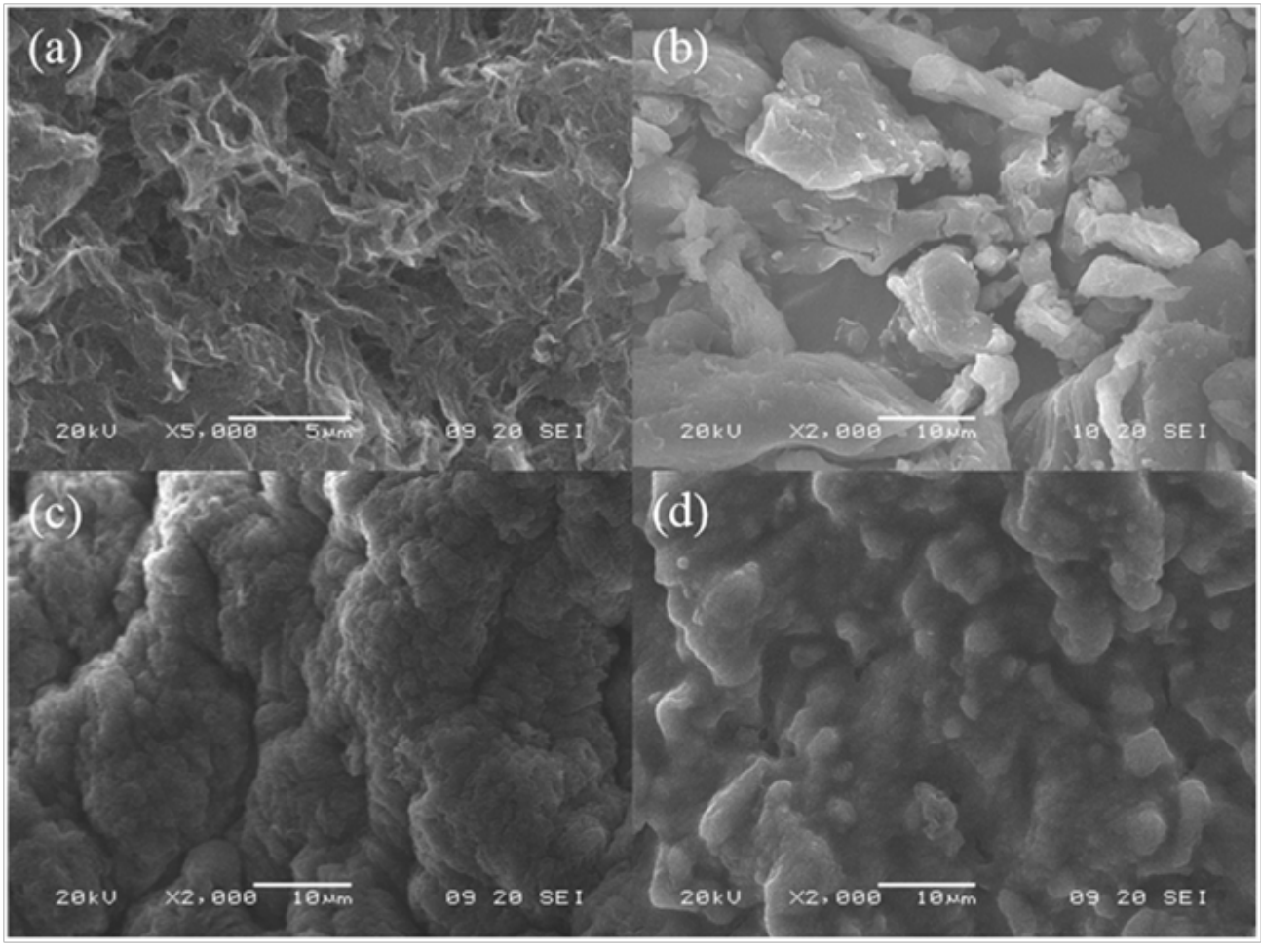

Figs 1A to D: Scanning Electron Microscopy (SEM) images of (A) GO; (B) Chitosan; (C) MCTS/GO before adsorption; (D) MCTS/GO after adsorption

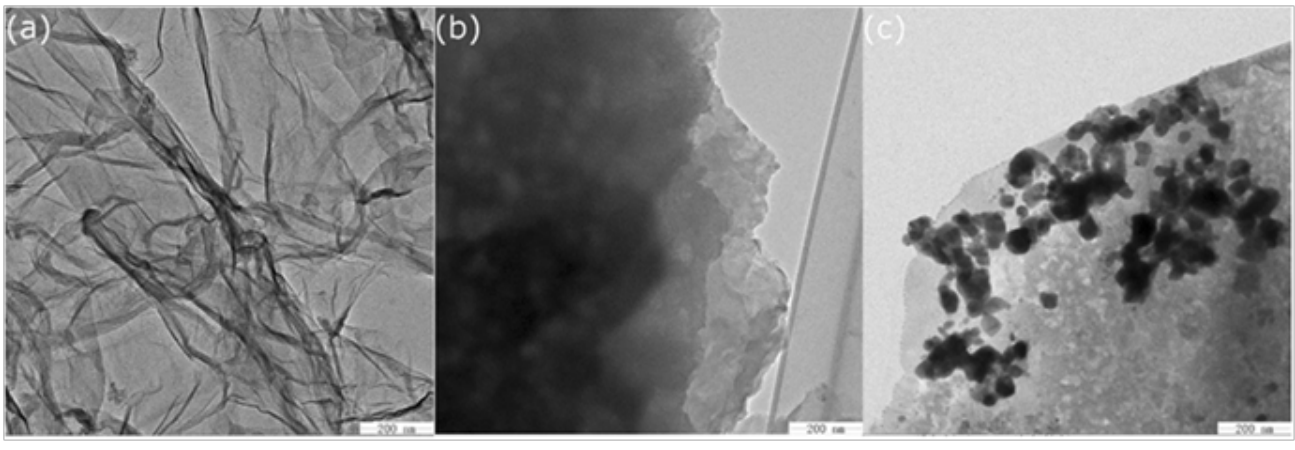

Figs 2A to C: TEM of the (A) GO; (B) CTS/GO before adsorption; (C) MCTS/GO after adsorption

MCTS/GO nanocomposites. The 2θ values were observed at 11.3°, 8.9°, 8.6°, and 7.8°, corresponding to the d-spacing values of 0.77, 0.98, 1.02, and 1.13 nm, respectively. The X-ray patterns of GO display the presence of a strong peak at 11.3° corresponding to the (001) reflection peak with a layer distance of 0.77 nm. Thus, the regular stacking of GO sheets was significantly altered by CTS chains which attached on the surface of the GO sheets, even though the structural features of GO remained largely unaltered.

3.3. Raman Spectra

Indeed, Raman spectroscopy provides a useful tool to characterize the carbon-based materials as shown in Figure 4. The characteristic bands of GO revealed by Raman spectra appeared, including the G band at (1601 cm–1) originated from the first-order scattering of the E2g phonons of the sp2-hybridized carbon atoms, the D band at (1351 cm–1) caused by a breathing mode of κ-point

phonons of A1g symmetry of the defects involved in the sp3-hybridized carbon bonds such as hydroxyl and/or epoxide bonds, and the 2D band at (2692 cm–1) which is much sensitive to stacking of graphene sheets. It is established that the G and 2D bands of single-layer graphene sheets are usually located at 1585 and 2679 cm–1, while for multi-layer graphene sheets, the positions of the G and 2D bands shift into lower and higher wavenumbers, respectively. Furthermore, the 2D/G ratios of single-, double-, triple-, and multi-layer graphene sheets are typically >1.6, 0.8, 0.30, and 0.07, respectively. Our results on the Raman spectra showed that the 2D/G ratios of the GO sheets and three different composite gels showed the values in the range of 0.12–0.14, suggesting the multi-layer nature of the presently prepared graphene sheets. Moreover, due to the origination of the G and D bands, the G/D peak intensity ratio is known as a measure of the sp2 domain size of graphene sheets containing sp3 and sp2 bonds. In addition, it was found that by forming the composite gels, the D/G ratios shifted from 0.97 to the values of 1.06, 1.19, and 1.20 with increasing of CTS concentration, respectively. This changein the D/G ratios can be attributed to the successful interaction and cross-linking of MCTS in the GO networks and the absence of the C–N bonds formed on the surface of the GO nanosheets.

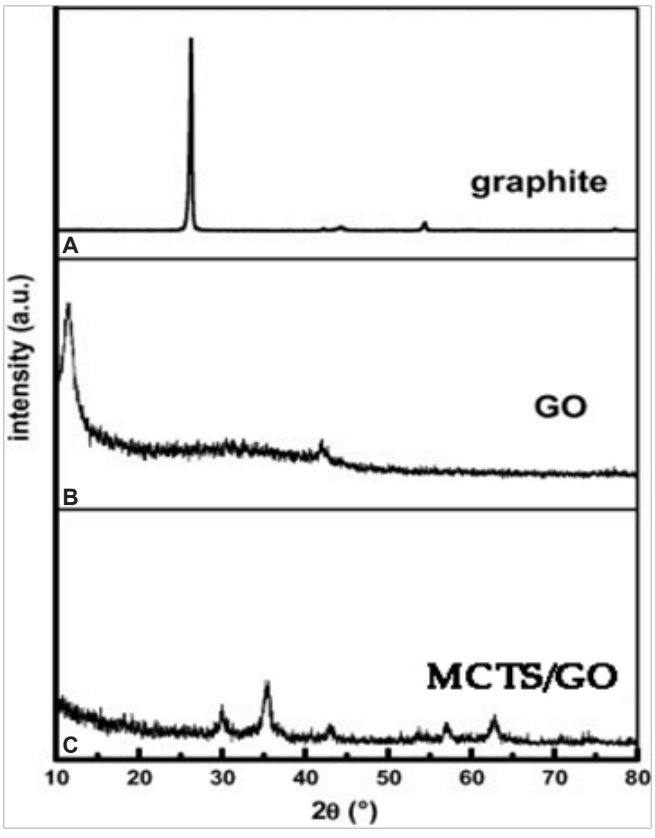

Figs 3A to C: X-ray diffraction patterns of (a) Graphite powder, b) Graphene oxide (GO) and (c) Magnetic chitosan graphene oxide nanocomposite (MCTS/GO).

3.4. FTIR Spectra

The mechanism of chemical reaction due to grafting of magnetic chitosan onto graphene oxide was studied using FTIR. The interaction of different functional groups during grafting were observed in all graphene samples through FTIR analysis is shown in Figure 5. As shown

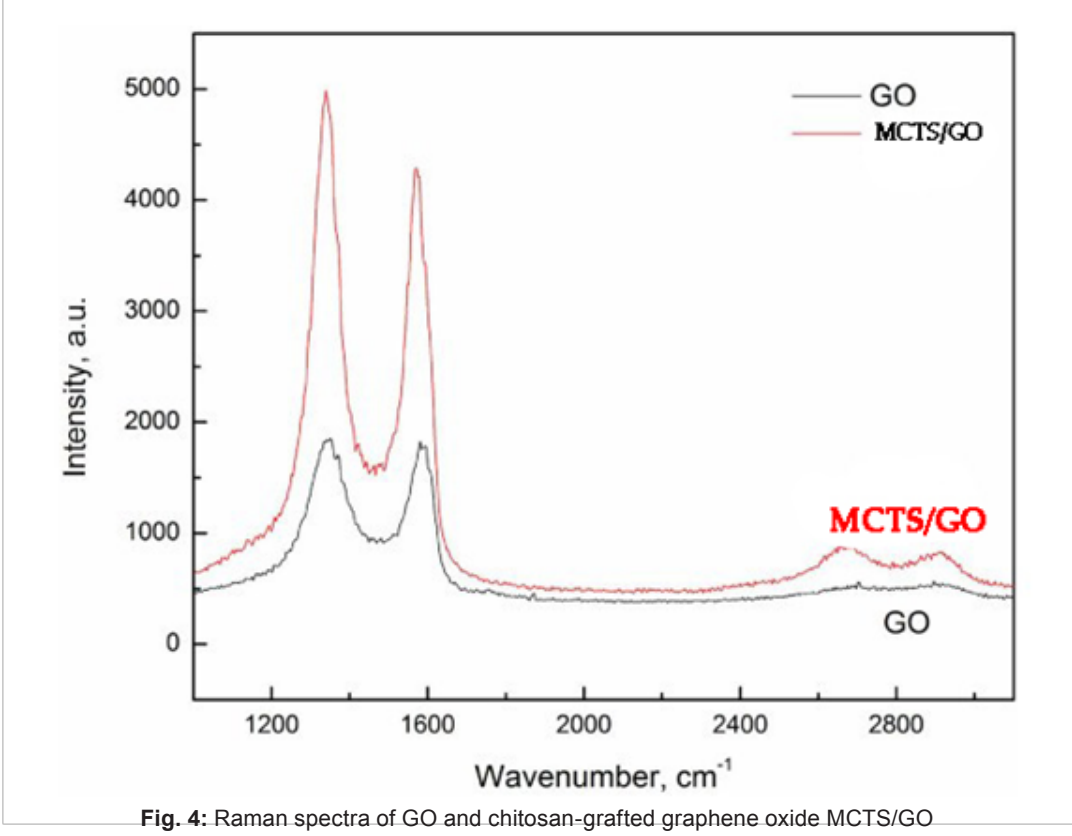

Fig. 4: Raman spectra of GO and chitosan-grafted graphene oxide MCTS/GO

in the Figure 5, a strong stretching vibration appeared at 3445 cm^{-1}, which is induced by the absorption peak characteristic of -OH bond; the absorption peak at 1384 cm–1 and 1399 cm–1 signaled the bending vibration of -CH^3; and the peak at 1633 cm^{-1} was originated by the vibration of C=C. Compared to the spectra of GO with CTS/GO, four new bands appear at 1085 cm^{-1}, 1031 cm^{-1}, 887 cm^{-1}, 816 cm^{-1}. The observed absorption peak for GO at 1399 cm^{-1} shown blue shifts after reaction with chitosan it was shifted to 1421 cm–1, that indicated the graphene oxide fully reacted with chitosan and the formation of the double network composite. However, when comparing CTS/GO spectra with MCTS/GO spectra, no significant new characteristic absorption peaks are observed but three absorption peaks at 1420 cm–1, 1083 cm–1, 883 cm–1 remarks a slight red shift occurrence. The absence of significant changes in FTIR spectra of CTS/GO and MCTS/GO implies the adsorption process is physical mechanism oriented. The FTIR spectrum of the MCTS/GO nanocomposite shows a combination of characteristics, which is similar to that of fine chitosan, and graphene oxide, which includes the broad absorption of band, is located at 3445.0 cm^{-1}, assigned to the mixture of the amine stretch from the chitosan to the OH groups in graphene oxide. The small peak at 1620.0 cm^{-1} illustrates the presence of the COOH groups from graphene oxide and is downshifted due to hydrogen bonding between the graphene oxide and hexatomic ring of the chitosan. On the other hand, the small peak at 1565.0 cm^{-1} indicates the presence of N-H bonding that is resulted from chitosan. The peak in the region about 1083.0 cm–1 is the indication of C–O–C stretching from the graphene oxide layers. Thus, FTIR results indicate the existence of strong interaction between chitosan and graphene oxide.

3.5. Thermo-gravimetric analysis results

The adsorption capacity of GO and MCTS/GO nanocomposite is determined by the content of oxygen-containing functional groups on the surface of GO and MCTS/GO, which could be determined by the Thermo-gravimetric analysis technique (TGA) via oxidative decomposition which was performed in nitrogen atmosphere from room temperature to 800 °C at a rate of 10 °C min–1. Figure 6 shows the representative TGA curves of GO (Figure 6a) and MCTS/GO (Figure 6b). As shown in Figure 6, there are three distinct loss of weight processes areas. The first weight loss is slight and occurred below 250 °C can be assigned to the evaporation of adsorbed water molecules. The second weight loss is marked highly and occurs from 250 to 350 °C, which can be ascribed to the removal of labile oxygen-containing functional groups such as epoxy, carboxyl and hydroxyl vapors from the sorbent surface.

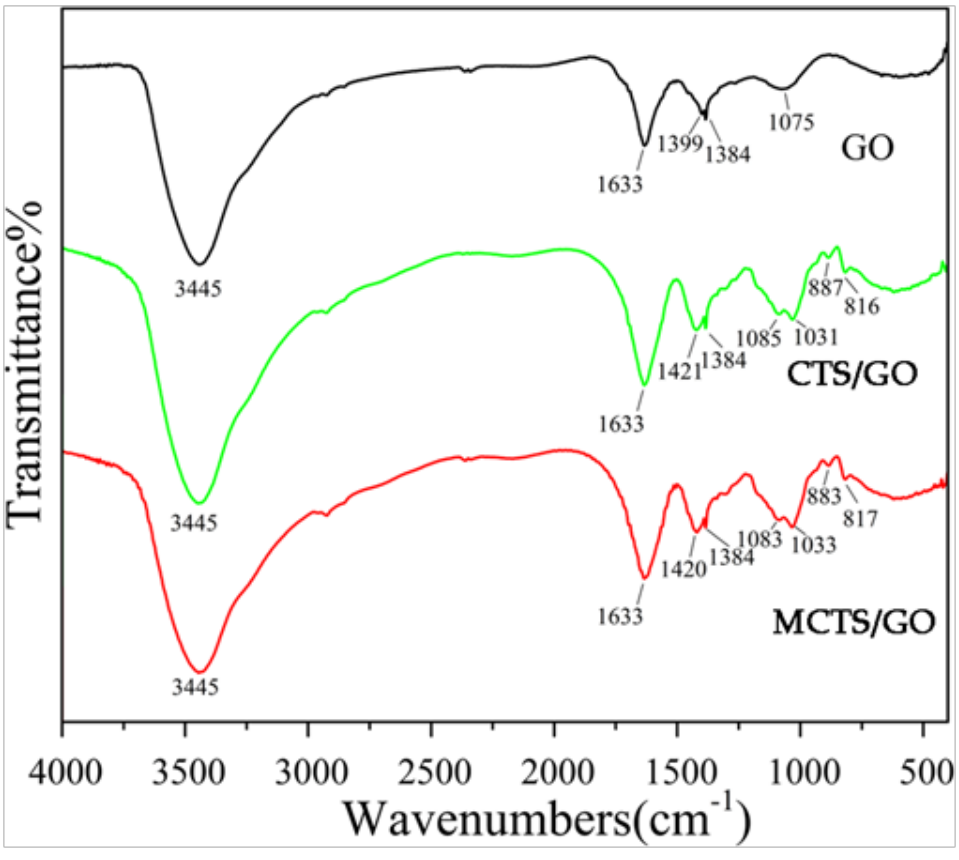

Figs 5A to C: Fourier transform infrared spectroscopy (FTIR) spectra of (A) graphine oxide (GO); (B) chitosan-grafted graphene oxide CTS/GO; (C) magnetic chitosan-grafted graphene oxide MCTS/GO nanocomposite

The third weight loss is slight and appeared from 350 to 700 °C, which can be attributed to the decomposition of the carbon skeleton. Noteworthy, the weight losses of MCTS/GO and GO at 250–350 °C are about 40.52% and 39.74%, respectively. These results indicate that both GO and MCTS/GO has abundant oxygen-containing groups on their surfaces, and thus MCTS/GO nanocomposites have higher oxygen-containing groups than GO.

3.6. Magnetic results

Figure 7 shows a hysteresis loop measured at room temperature of (a) Fe_3O_4 and (b) MCTS/GO nanocomposite at room temperature. As shown, the GO–Fe_3O_4 exhibits no remanence (magnetization left behind in a ferromagnetic material) or magneticcoercivity at room temperature, revealing its superparamagnetic characteristics. Due to the micro scale dimension of Fe_3O_4 particles being modified on CTS/GO nanocomposite, the saturation magnetization of MCTS/GO nanocomposite is 9 emu g–1, but it is sufficient for magnetic separation by an ordinary magnet. Figure 7b shows photograph of MCTS/GO adsorption and the separation under an external magnetic field. A handle magnet within 1–2 min can collect the MCTS/GO dispersed in aqueous solution easily and the aqueous solution becomes colorless, and MCTS/GO can be readily re-dispersed with slight shake after removing the magnetic field. Hysteresis loop results reveal that MCTS/GO has characteristics of good magnetic separation, suggesting that MCTS/GO can be used as a magnetic adsorbent for accumulation and removal of organic dyes contaminants from aqueous solutions.

3.7. UV-Vis spectra

Figure 8 shows the UV-Vis absorption spectra of GO and MCTS/GO nanocomposite. GO displays a characteristic peak at 228 nm corresponding to $\pi \rightarrow \pi^*$ transitions of aromatic C__C bonds, while for MCTS/GO nanocomposite the absorption peak blue shifts to 224 nm, indicating that MCTS particles are covalently attached onto GO surface. The spectra of MCTS/GO nancomposite is shown in Figure 8, after samples dispersed in water with sonication and 24 h kept to rest. This shift in absorption maxima might be attributed to the formation of particles in the nano scale. This also confirm the strong covalent interaction between GO and Chm where the active ester group of GO might have reacted with the amine groups on Chm, forming an amide bond between GO and Chm. Optical analysis shows the band gap energy of GO to be 1.02 eV and that of the nanocomposite to be 1.08 eV. Since these values are within the range of semiconductor indicating that the conductivity of the constituents are retained in the composites thus enabling their application in the field of accumulation. The shown peak related to the π–π^* transitions at 228 nm and the shoulder at 300 nm due to n–π^* transition are clear and more intensive

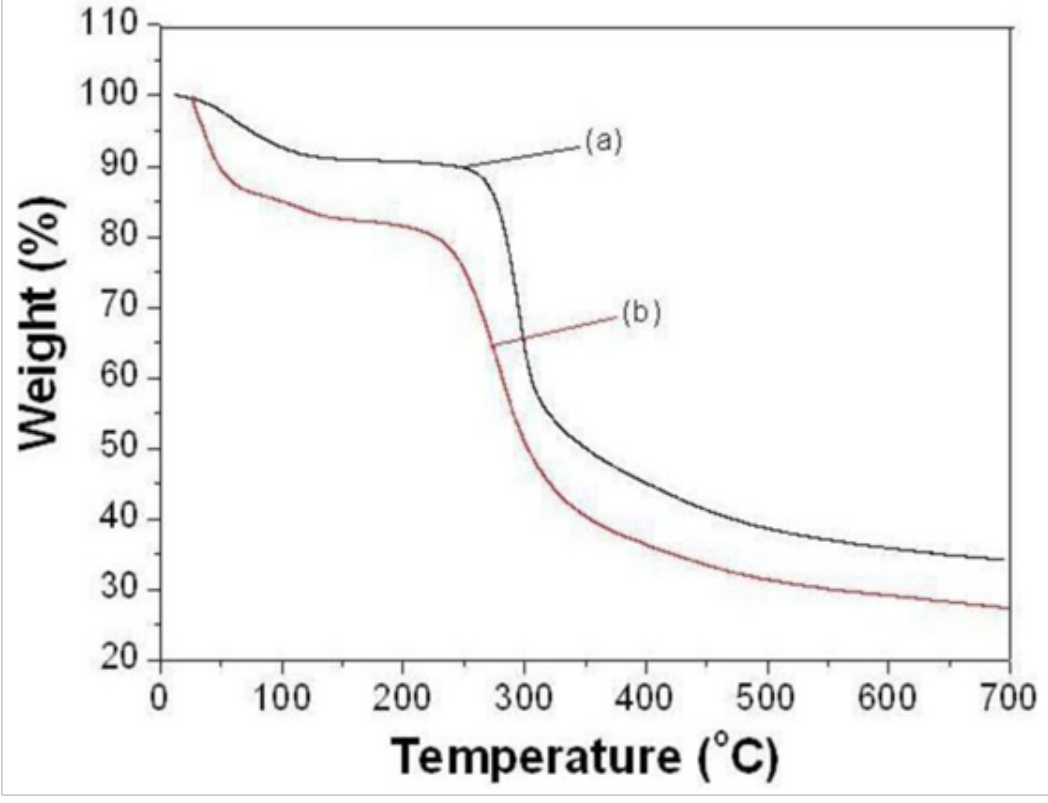

Figs 6A and B: Thermogravimetric analysis (TGA) of (a) graphine oxide (GO) and (b) MCTS/GO nanocomposite

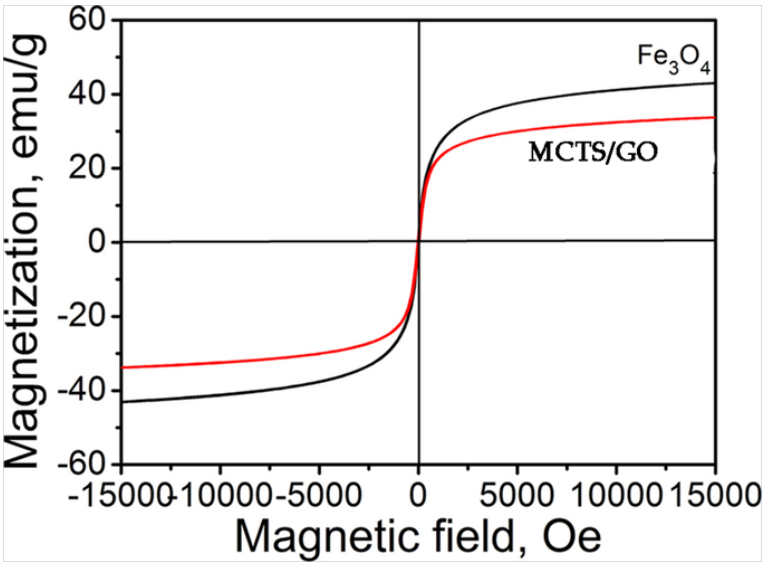

Figs 7A and B: Hysteresis loop of (A) Fe3O4and (B) MCTS/GO nanocomposite at room temperature

in MCTS/GO nanocomposite than in GO spectra, giving evidence that better dispersion is reached even maintaining at rest for 24 h. In addition, it is evident than MCTS/GO is the grafted sample that maintains absorption due to better dispersion than the GO samples.

3.8. Adsorption capacity of MCTS/GO nanocomposite with different weight ratios of GO and magnetic chitosan

The effect of different weight ratios of GO and magnetic chitosan on the adsorption property of the nanocomposite was investigated. It can be seen from Figure 9 that pure chitosan have a lower adsorption capacity for CY. The adsorption capacity is 107.4 mg/g, which is higher than powdered activated carbon (91 mg/g), suggesting that chitosan is a good adsorbent. Moreover, the chitosan act as the supporter to form composite fibres on the GO sheet to improve the stability and easy separation of the GO. As 50 wt % GO is mixed with chitosan, the adsorption capacity of the MCTS/GO nanocomposite increases sharply and reaches 352.7 mg/g. By further increasing the weight ratio of GO, the adsorption capacity of the fibres also increases correspondingly and reaches a maximum of 382.4 mg/g for a weight ratio of GO and chitosan at 5:1. For the pure GO, the adsorption capacity is 398.8 mg/g. Compared to the pure GO, although the adsorption capacity of MCTS/GO nanocomposite fibres is decreased, the chitosan and GO composite have improved stability and are easily separated from solution, which have great impact to the real application. Due to the insufficient formation of the MCTS/GO nanocomposite (5:1) and only a slight difference in adsorption capacity between two samples with weight ratios of 4:1 and 5:1, the MCTS/GO nanocomposite with the weight ratio of GO and MCTS at 4:1 are chosen in the following adsorption experiments.

Indeed, there are numerous studies data on the accumulation and removal of water-soluble dye with GO as adsorbent. For example, Yang et al group have reported that GO can be directly utilized for the removal of methylene blue (MB) from wastewater with excellent adsorption capability performance (~714 mg/g) (Yang, 2012). Moreover, Liu et al group demonstrated that a three-dimensional (3D) graphene oxide nano composite sponge could accumulate and remove dyes such as MB with high efficiency from water (Zhang et al, 2011). In addition, Zhang et al. showed that GO prepared via modified Hummer's method could adsorb MB very quickly but hardly release the dyes back (Zhang et al, 2011). Indeed, Deng et al. (Deng et al, 2016) has reported that GO possesses excellent adsorption efficiency of 351 mgg-1 for Methylene blue (MB) based on Langmuir isotherm which is much higher than activated carbon owing to larger surface area in the former, thus playing important role in adsorption phenomena. In addition, similar comparative study of functionalized carbonaceous materials as adsorbents, specially, activated carbon (AC), graphene oxide (GO) and multi-walled carbon nanotubes (CNTs), for the removal of methylene blue dye from aqueous solution carried out by Li et al. (Pal and Majumdar, 2016). The adsorption capacities of MB onto AC, GO and CNTs were 270.27, 243.90 and 188.68 mg/g, respectively and with followed the order of capacity AC>GO>CNTs.

3.9. Adsorption kinetics

Indeed, several models can be carried out to understand the adsorption property and to predict the mechanism

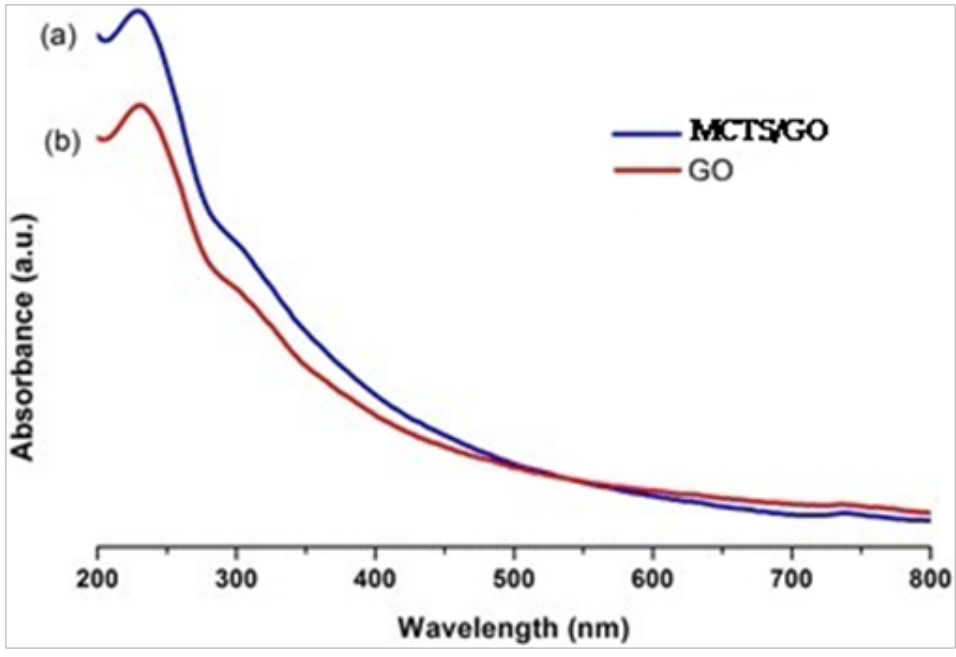

Figs 8A and B: The UV-Vis spectra of (A) GO; (B) MCTS/GO nanocomposite after samples dispersed in water with sonication and 24 h kept to rest

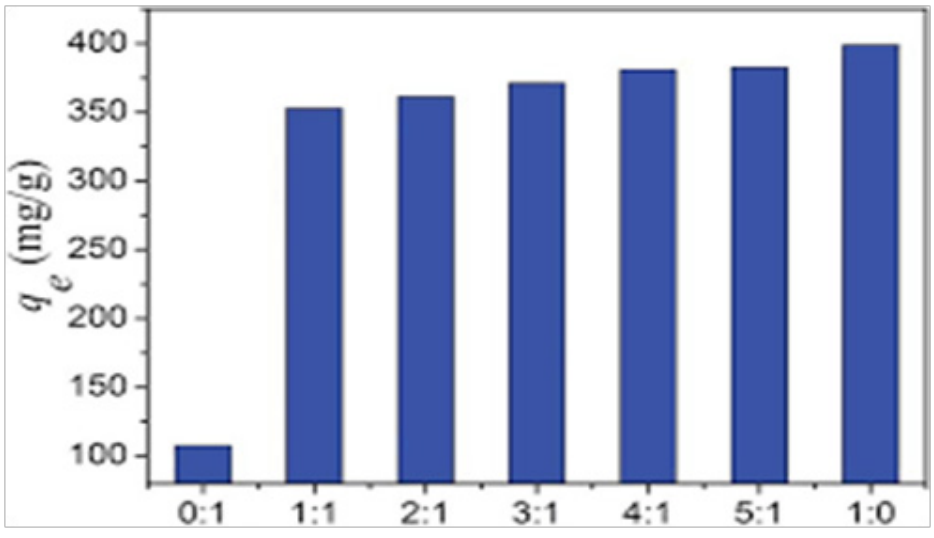

Fig. 9: Comparison of the adsorption capacity (qe) of the with different weight ratios of GO and magnetic chitosan (initial CY concentration: 180 mg/L, pH: 6.0, dosage: 20 mg, and temperature: 298 K)

of CY adsorption onto an MCTS/GO nanocomposite adsorbent. In order to design a fast and effective model, investigations are made on adsorption rate. For the examination of the controlling mechanisms of adsorption process, such as chemical reaction, diffusion control and prompt mass transfer, several kinetics models are used to test the experimental data. Kinetics experiments were performed by adding 5.0 mg of new prepared MCTS/GO nanocomposite to 5.0 mL aqueous solution containing 100, 200, 300 and 400 mg L^{-1} CY at room temperature. The results in Figure 10 shows the effect of adsorption time on the removal of CY by MCTS/GO nanocomposite. The result displays that a fast adsorption process occurs during the first few minutes and then reaches equilib-

Table 1: Comparison of the adsorption capacities of various adsorbents for CY

Adsorbents	*Adsorption capacity (mg g^{-1})*	*Contact time (min)*	*Ref.*
Bottom ash	18.08	180	Mittal et al. (2010)
De-oiled soy	8.33	180	Mittal et al. (2010)
FC	57.3	180	Mittal et al. (2010)
GC	44.6	180	Mittal et al. (2010)
Beads	61.5	180	Nurchi et al. (2014)
GO	680.3	30	Yongmeiet al. (2015)
Fe_3O_4	63.94	30	Yongmeiet al. (2015)
GO–Fe_3O_4	359.71	30	Yongmeiet al. (2015)
MCTS/GO	370.57	60	This worka
MCTS/GO	700.6	60	This worb

a: at 150 mg/L CY and a: at 300 mg/L CY

rium. The result indicates that the adsorption equilibrium time is about 30 min for all the concentrations, which can be attributes to the adequate free adsorptive sites and a high concentration gradient. This rapid adsorption indicates that the adsorption occurs mainly on the surface of MCTS/GO nanocomposite adsorbent and not on the bulk of the nanocomposite material.

3.10. Effect of Adsorbent and Dye Doses

The effect of adsorbent dose on the accumulation and removal of CY by MCTS/GO nanocomposite at initial CY concentration of 150 mg L^{-1}, is demonstrated in Figure 11. Results illustrated describe that CY removal increases upto a certain limit and then it remains almost constant. With increase in the adsorbent dose from 0.1 to 1.2 g, thus dye accumulation increases from 83–95% and 60–82% for MCTS/GO and GO, respectively. It is evident that the increase in accumulation with adsorbent dosage can be attributed to increased adsorbent surface area and availability of more adsorption sites on MCTS/GO nanocomposite surface.

Figure 12 shows plots of the equilibrium accumulation capacity of MCTS/GO nanocomposite and the percentage removal of CY versus the initial concentration of CY. It was observed that the equilibrium adsorption capacity increases with increasing initial dye concentration, indicating that a higher initial concentration of CY can enhance the adsorption capacity process, although the percentage removal of CY decreases with an increase in the initial concentration. The maximum adsorption capacity of the MCTS/GO nanocomposite adsorbent at CY concentration of 300 mg/L is 233.40 mg/g. The increasing accumulation capacity of the adsorbent with increasing CY concentration may be due to higher collision probability between CY ions and adsorbent functional groups on the surface of MCTS/GO nanocomposite. Moreover, variation in the extent of adsorption may also be because at the initial stage, all active functional groups sites of the adsorbent surface are vacant and the CY dye concentration gradient is relatively high.

3.12. Effect of pH

The percentage of dye adsorption at different pH is shown in Figure 13. The influence of initial pH on adsorption efficiency was evaluated in terms of adsorption capacity. The initial pH of CY dye solution plays an important role particularly on the accumulation capacity by influencing the chemistry of both CY dye molecule and MCTS/GO adsorbents in aqueous solutions. The color of CY in aqueous solution is red at pH around 7. The color of CY changes to dark blue at acid pH and to red at alkaline pH (10–12), but this red color is slightly different from original red at the neutral pH. The CY dye exists as an anionic form at basic pH and as a cationic form at acid pH As illustrated in the Figure 13, when pH value of dye solution increased from 2 to 12, the percentage of dye adsorption sharply reduced from 94 to 73% in case of MCTS/GO and 75 to 51% in case of CY. At pH 2.0 a significantly high-electrostatic attraction exists between the positively charged surface of the adsorbent and anionic dye. As the pH of the system increases, the number of negatively charged functional groups sites increases and the number of positively charged sites decreases. Another possibility is that the negatively charged surface site on the adsor-

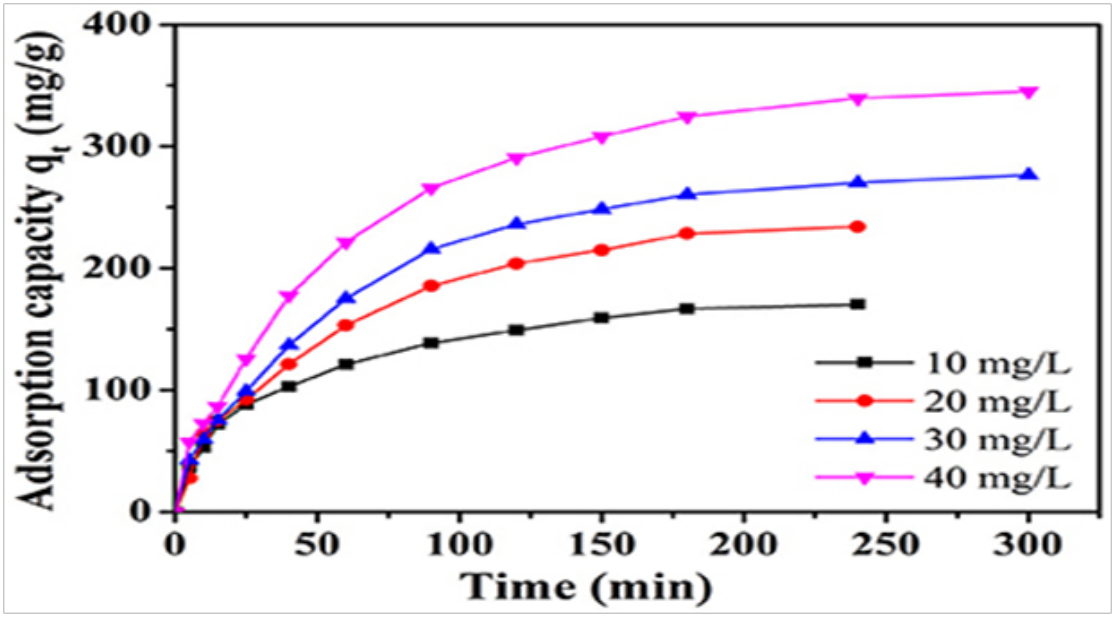

Fig. 10: Effect of adsorption time on the adsorption capacity for CY onto MCTS/GO nanocomposite at different initial CY concentration (100 mg L^{-1}, 200 mg L^{-1}, 300 mg L^{-1} and 400 mg L^{-1}) at room temperature; dosage of MCTS/GO nanocomposite was 5.0 mg

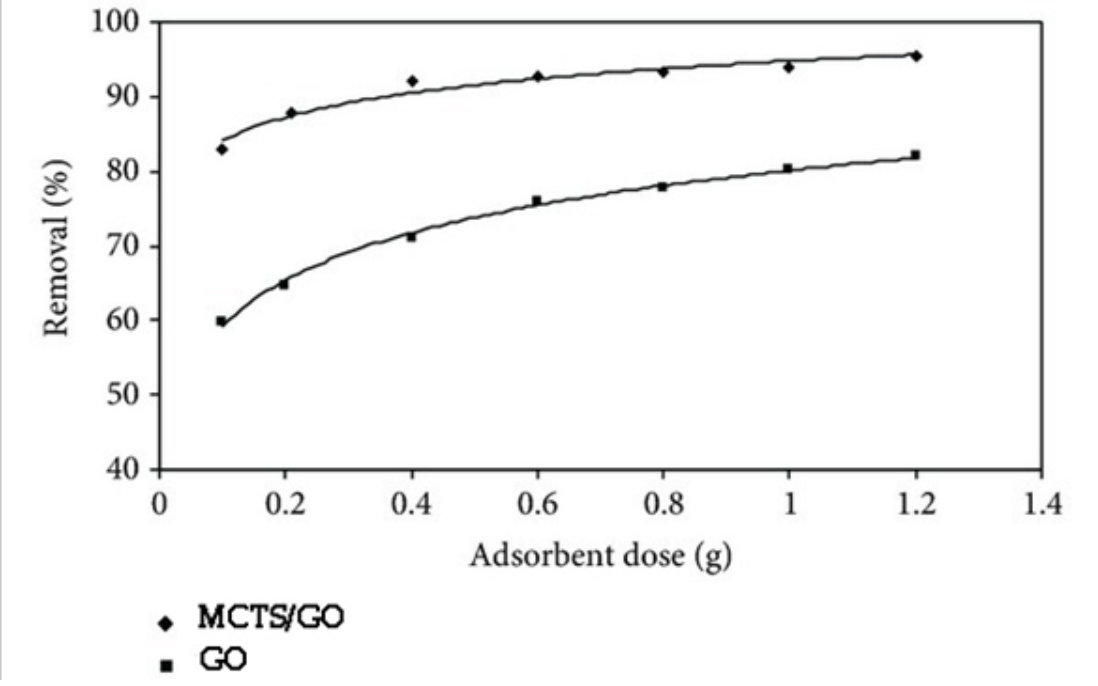

Fig. 11: Effect of adsorbent dose on adsorption of CY onto MCTS/GO nanocomposite and GO (CY concentration of 150 mg L−1, pH = 7.0)

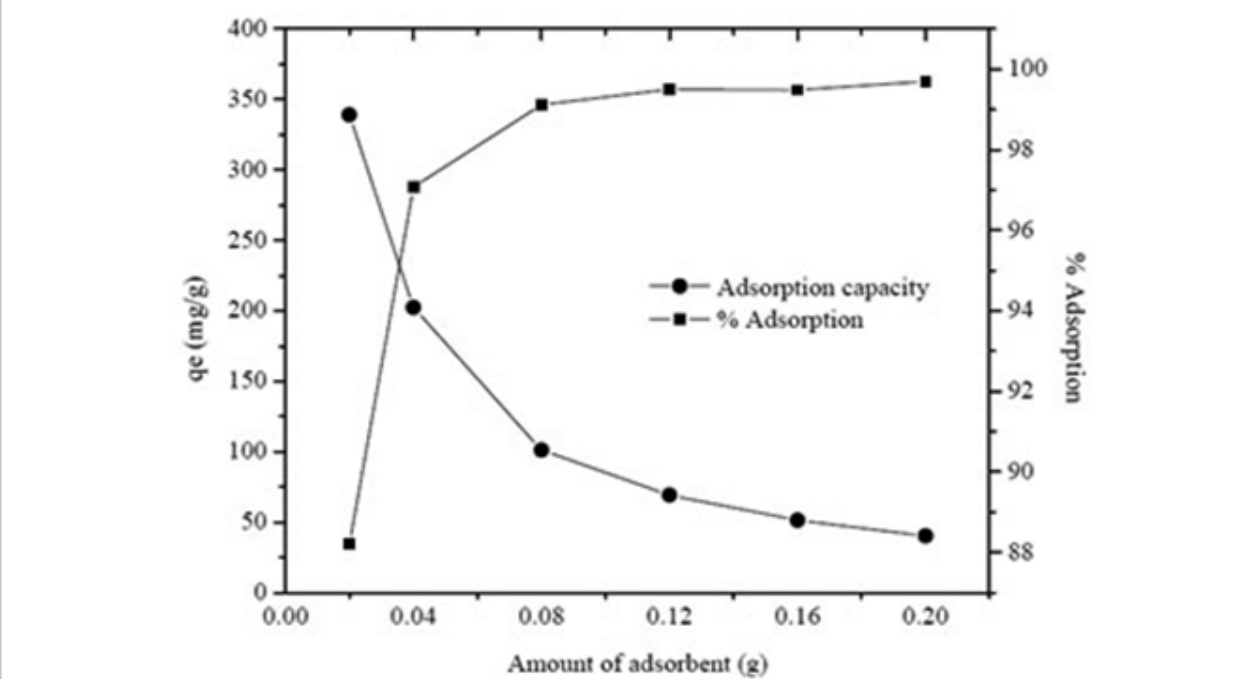

Fig.12: Effect of adsorbent dosage on adsorption of CY onto MCTS/GO nanocomposite. (CY concentration of 150 mg L−1, pH = 7.0)

bent does not favor the adsorption of dye anions due to the electrostatic repulsion. In addition, lower adsorption of CY at alkaline pH is due to the presence of excess ions competing with the dye anions for the adsorption sites. Nevertheless, significant adsorption of anionic dye on the adsorbent still occurred above because a chemical interaction occur between the dye and MCTS/GO. The pH of an aqueous solution is generally said to be a very critical parameter affecting the adsorption process due to the functional groups of both the adsorbed functional groups and the adsorbent particles. Hydrogen ions (H+) in the solution are directly involved in the adsorption process at the active sites of the adsorbent.

3.13. Effect of initial CY concentration and temperature

The effect of the initial concentration of CY is a very important parameter for adsorption studies because it can overcome all mass transfer restrictions between the aqueous and solid phases. The effect of the initial dye concentration factor depends on the immediate

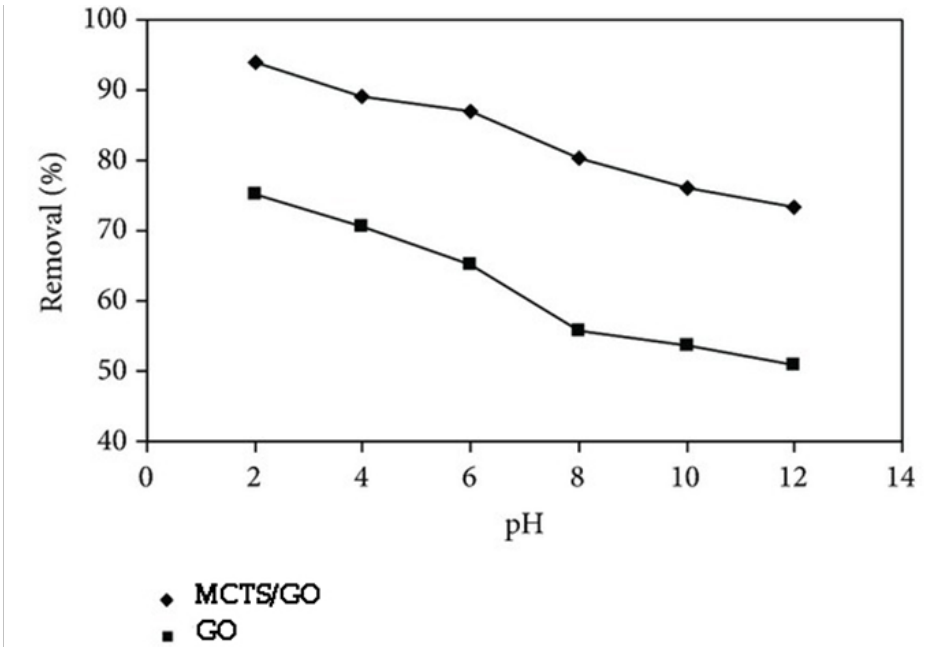

Fig. 13: Effect of pH values on the adsorption of CY by MCTS/GO and GO (sorbent dose = 5 g L^{-1}, CY concentration 50 mg L^{-1})

relation between the dye concentration and the available binding functional group sites on an adsorbent surface. The amount of CY adsorbed increased with the increase in the concentration CY. This indicates that the initial concentration plays an important role, which provided the necessary driving force to overcome the resistances to the mass transfer of CY between the aqueous and the solid phases. The interaction between adsorbate and adsorbent was also found to enhance with the increase in the initial concentration. Thus, it can be concluded that higher initial concentration enhances the adsorption uptake of CY. The initial CY concentration and temperature are important factors to determine the process of adsorption. Figure 14 narrates that the adsorption capacity increases with increasing the initial CY concentration.

3.14. Effect of Ionic Strength

In order to study the ionic strength effect on adsorptive removal of CY by MCTS/GO nanocomposite different concentrations of NaCl and KCl were added (0.01–0.05 M). Figure 15 shows that increase in ionic strength causes increase in the adsorption of CY. It was observed that salt addition increases the aggregation of dye molecules and decreases the solubility. Thus, an increase in aggregation promotes the adsorption of dye molecules (Mittal et al, 2010; Alonso, 2014; Yongmie Hao et al, 2015). Thus, the increase in ionic strength increases the positive charge of the adsorbent MCTS/GO nanocomposite surface thus increases the electrostatic attraction between dye (CY) and adsorbent. Thus, increase in ionic strength was found to have an increase in adsorption of CY.

3.15. Regeneration of CGO fibre

Regeneration and reuse of adsorbents is a good factor for evaluating the economy in commercial applications. After adsorption of the CY on MCTS/GO nanocomposite fibre, the mixture was added into 0.2 M NaOH or 0.2 M HCl solution, and was stirred for 3 h. The MCTS/GO nanocomposite was washed with deionised water two times to remove the residual NaOH or HCl solution. Then, the MCTS/GO nanocomposite was regenerated through vacuum drying at 323 K and reused for adsorption. The relative capacity for each cycle was calculated. As Figure 16 shows, the NaOH solution more effectively regenerated the CGO fibre, with 94% capacity retention after three cycles. Therefore, the MCTS/GO nanocomposite fibre is a stable, cost effective, and effective adsorbent for CY removal. Figure 16 shows, the NaOH solution more effectively regenerated the CGO fibre, with 94% capacity retention after three cycles. Thus, the MCTS/GO nanocomposite fibre is a stable, cost effective, and effective adsorbent for CY removal.

In this work, the results of the research have shown that MCTS/GO nanocomposite as an inexpensive adsorbent was used for the accumulation and removal of Chrysoidine Y (CY) from aqueous solutions. The fast adsorption at initial contact time can be attributed to the accessibility of large number of the unfilled sites on the sorbent MCTS/GO nanocomposite surface at the early step of the adsorption process and the adsorption sites were gradually occupied by the pollutant dye molecules as the contact time was increased. The removal rate of CY was increased with increase of the solution pH from 2 to 12 due to the increase in the magnitude of the electrostatic

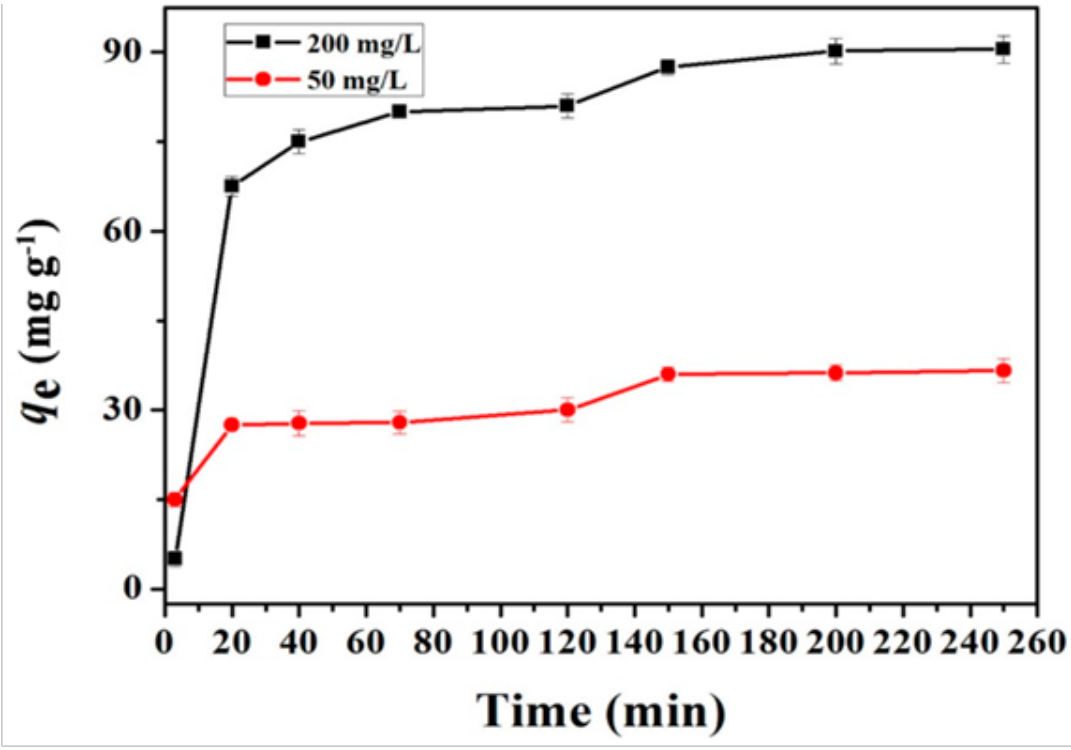

Fig. 14: Effect of initial CY concentration and temperature on the adsorption of CY onto MCTS/GO nanocomposite (pH: 6.0, dosage: 20 mg)

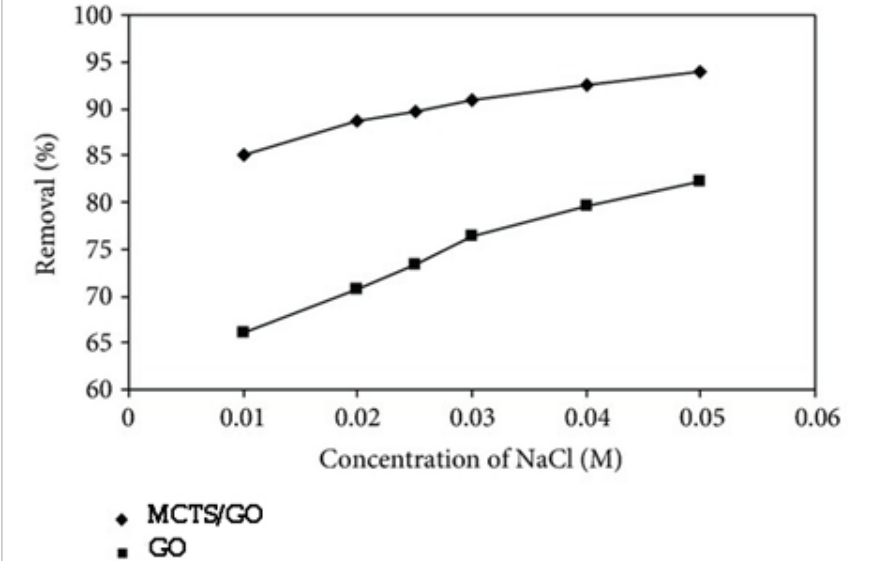

Fig. 15: Effect of ionic strength on sorption of CY by MCTS/GO nanocomposite and GO (sorbent dose = 1 g L−1, CY concentration 50 mg L−1, pH = 7.0)

attractions between CY and positive charge adsorption sites on MCTS/GO nanocomposite. The adsorption of CY on the MCTS/GO nanocomposite surface is primarily influenced by the surface charge on the adsorbent. This finding is in agreement with the results of the study of Mittal et al. for the biosorption of CY by Bottom ash and De-oiled soy, Nurchi et al. for the biosorption of CY by Beads and Yongmei et al for the biosorption of CY by Fe_3O_4 , GO and GO–Fe_3O_4. They showed that the sorption of CY is weak in acidic medium.

CONCLUSIONS

A novel and efficient MCTS/GO nanocomposite fibre adsorbent with enhanced adsorption capacity for the removal of CY was prepared by wet-spinning technique. The adsorption capacity was found to increase with increasing solution pH, initial CY concentration, and temperature. The maximum adsorption capacity of CY onto the MCTS/GO nanocomposite fibres was 480.77 mg/g. The kinetic adsorption followed pseudo-

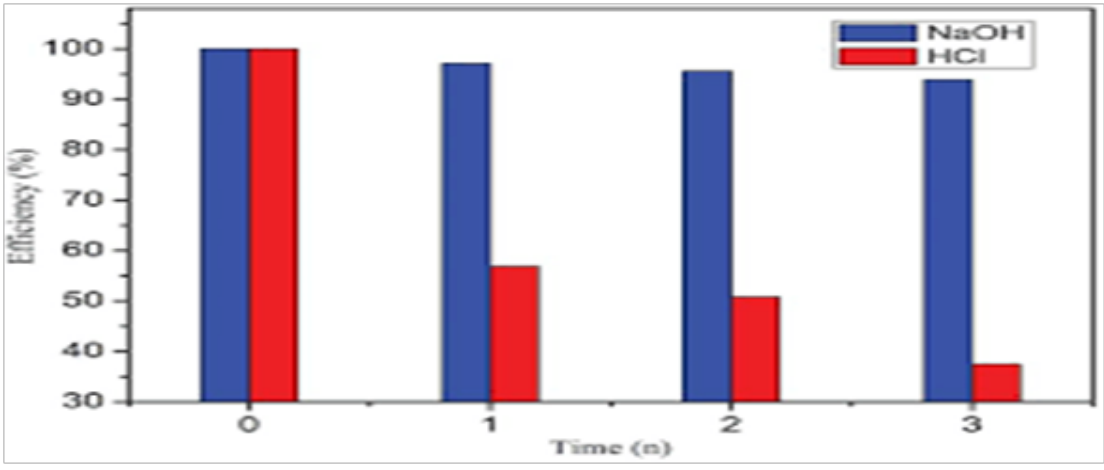

Fig. 16: Regeneration and reuse of MCTS/GO nanocomposite. The labels of NaOH and HCl represent the relative capacity after NaOH solution and HCl solution washing, respectively (initial CYconcentra-tion: 150 mg/L, dosage: 20 mg, temperature: 298 K, and pH: 6)

second-order kinetic model. Furthermore, the MCTS/GO nanocomposite fibres can be effectively regenerated with a dilute NaOH solution and still retain high adsorption capacity after three cycles. The investigation proves that the MCTS/GO nanocomposite fibre is an efficient and cost-effective adsorbent for practical application in the treatment of CY dye wastewaters.

REFERENCES

1. Alonso R, Biesuz G, Alberti M.I, Pilo N, Spano G. (2014) Sanna Sorption of chrysoidine by row cork and cork entrapped in calcium alginate beads. *Arab. J. Chem*. 7 (1):133-138
2. Aksu Z. (2005) Application of biosorption for the removal of organic pollutants: a review. *Process Biochem*. 40:997-1026.
3. Aksu Z. (2005) Application of biosorption for the removal of organic pollutants: a review. *Process Biochem*. 40:997-1026.
4. Brindley L. (2018). New solution for dye wastewater pollution. *Chemistry World*. Retrieved, 07-08.
5. Coasne B, Alba-Simionesco C, Audonnet F, et al (2011). Adsorption, structure and dynamics of benzene in ordered and disordered porous carbons. *Phys. Chem. Chem. Phys*. 13:3748-3757.
6. Coasne B, Alba-Simionesco C, Audonnet F, et al (2011). Adsorption, structure and dynamics of benzene in ordered and disordered porous carbons. *Phys. Chem. Chem. Phys*. 13: 3748-3757.
7. Das T K, Prusty S (2013). Graphene-based polymer composites and their applications. *Polym Plast Technol Eng*. 52: 319-331.
8. Deng XZ, Wang YW, Peng JP, et al (2016). Surface area control of nanocomposites Mg(OH)2/graphene using a cathodicelectrodeposition process: High adsorption capability of methyl orange. *RSC Adv*. 6: 88315-88320.
9. Du QJ, Sun JK, Li YH, et al (2014). Highly enhanced adsorption of congo red onto graphene oxide/chitosan fibers by wet-chemical etching off silica nanoparticles. *Chem. Eng J*. 245:99-106.
10. Du B. (2015). Removal of dissolved organic carbon (DOC) from high DOC and hardness water by chemical coagulation: relative importance of monomeric, polymeric, and colloidal aluminum species. *Separ. Sci. Technol*. 50:2075-2085.
11. Du QJ, Sun JK, Li YH, et al (2014). Highly enhanced adsorption of congo red onto graphene oxide/chitosan fibers by wet-chemical etching off silica nanoparticles. *Chem. Eng. J*. 245:99-106.
12. Du QJ, Sun JK, Li YH, et al (2014). Highly enhanced adsorption of congo red onto graphene oxide/chitosan fibers by wet-chemical etching off silica nanoparticles. *Chem. Eng. J*. 245: 99-106.
13. Du J, Cheng H M (2012). The fabrication, properties, and uses of graphene/polymer composites. *Macromol. Chem. Phys*. 213: 1060-1077.
14. Draget K I, Skjåk-Bræk G, Smidsrød O (1997). Alginate based new materials. Int J *Biol. Macromol*. 21:47–55.
15. Dreyer DR, Park S, Bielawski CW, et al (2010). The chemistry of graphene oxide. *Chem. Soc. Rev*. 39:228–240.
16. El-Naas MH, Al-Muhtaseb SA, Makhlouf S (2009). Biodegradation of phenol by pseudomonas putida immobilized in polyvinyl alcohol (PVA) gel. *J Hazard. Mater*. 164:720-725.
17. Gulshan F, Yanagida S, Kameshima Y, et al (2010). Various factors affecting photodecomposition of methylene blue by iron-oxides in an oxalate solution. *Water. Res*. 44:2876-2884.
18. Huang X, Qi X, Boey F, Zhang H (2012). Graphene-based composites. *Chem. Soc. Rev*. 41:666-686.
19. Jagiello J, Judek J, Zdrojek M, Aksienionek M and Lipinska L (2014). Production of graphene composite by direct graphite exfoliation with chitosan. *Materials Chemistry and Physics*. 148(3): 507=511,
20. Kim H, Abdala AA, Macosko CW (2010). Graphene/polymer nanocomposites. *Macromolecules*. 43:6515=6530.
21. Krishnan D, Kim F, Luo J, Cruz-Silva R, Cote L J, Jang H D, Huang J (2012). Energetic graphene oxide: Challenges and opportunities. *Nano Today*. 7:137-152.
22. Kuang D, Hu W B (2013). Research progress of graphene composites. WujiCailiaoXuebao. *J. Inorg. Mater*. 28:235-246.
23. Kumar RV, Ghoshal AK, Pugazhenthi G. (2015). Fabrication of zirconia composite membrane by in-situ hydrothermal technique and its application in separation of Kyzas G Z, Bikiaris D N, Seredych M, Bandosz T J, Deliyanni E A (2014) Removal of dorzolamide from biomedical wastewaters with adsorption onto graphite oxide/poly(acrylic acid) grafted chitosan nanocomposite. *Bioresour. Technol*. 152:399-406.

24. Kyzas G Z, Deliyanni E A, Matis K A (2014). Graphene oxide and its application as an adsorbent for wastewater treatment. *J. Chem. Technol. Biotechnol*. 89:196-205.
25. Kyzas G Z, Travlou N A, Deliyanni EA (2014). The role of chitosan as nanofiller of graphite oxide for the removal of toxic mercury ions. *Colloids Surf. B Biointerfaces*. 113:467-476.
26. Liang YY, Wu DQ, Feng XL, et al. (2009). Dispersion of graphene sheets in organic solvent supported by ionic interactions. *Adv. Mater*. 21:1679-1683.
27. Liu T, Li YH, Du QJ, et al. (2012) Adsorption of methylene blue from aqueous solution by graphene. *Colloid Surf B: Biointerfaces*. 90:197-203.
28. Li YH, Du QJ, Liu TH, et al. (2011). Preparation of activated carbon from enteromorphaprolifera and its use on cationic red X-GRL removal. *Appl. Surf. Sci*. 257:10621-10627.
29. Li YH, Du QJ, Liu TH, et al (2011). Preparation of activated carbon from enteromorphaprolifera and its use on cationic red X-GRL removal. *Appl. Surf. Sci.* 257:10621-10627.
30. Li Y, Du Q, Liu T, et al (2013). Methylene blue adsorption on graphene oxide/calcium alginate composites. *Carbohydr. Polym*. 95:501-507.
31. Li X, Zhou H, Wu Wm Wei S, Xu Y and Kuang Y (2015) Studies of heavy metal ion adsorption on Chitosan/Sulfydryl-functionalized graphene oxide composites. *Journal of Colloid and Interface Science*. 448:389-397.
32. Layek R K, Samanta S and Nandi A K (2012). Graphene-sulphonic acid/chitosan nanobiocomposites with tunable mechanical and conductivity properties. *Polymer*. 53(11): 2265-2273.
33. Liu F, Chung S, Oh G, et al. (2012). Three-dimensional graphene oxide nanostructure for fast and efficient water-soluble dye removal. *ACS Appl. Mater. Interfaces*. 4(2):922-927.
34. Malafaya P B, Silva G A, Reis R L (2007). Natural-origin polymers as carriers and scaffolds for biomolecules and cell delivery in tissue engineering applications. *Adv. Drug. Deliv. Rev.* 59:207-233.
35. Meral K, Metin O (2014). Graphene oxide-magnetite nanocomposite as an efficient and magnetically separable adsorbent for methylene blue removal from aqueous solution. *Turk. J. Chem*. 38:775-782.
36. Mittal A, Mittal J, Malviya A, Gupta VK (2010). Removal and recovery of Chrysoidine Y from aqueous solutions by waste materials. *Journal of Colloid and Interface Science*. 344(2):497-507.
37. Parida, KM, Sahu, S, Reddy KH, et al (2011). A kinetic, thermodynamic, and mechanistic approach toward adsorption of methylene blue over water-washed manganese nodule leached residues. *Ind. Eng. Chem. Res*. 50:843-848.
38. Park S, Ruoff RS (2009). Chemical methods for the production of graphenes. *Nat. Nano. technol*. 4:217-224.
39. Pal S, Majumdar D (2016). Book title modern trends in chemical sciences. Edited Dr. Kamala Mitra. Chapter on: Adsorption and removal of soluble methylene blue dye from water by sorbefacientgraphene oxide. 19-27.
40. Pati MK, Pattojoshi P and Roy GS (2015). Fabrication and characterization of graphene based nanocomposite for electrical properties. *Advances in Materials Physics and Chemistry*. 5(1):22-30.
41. Rinaudo M (2008). Main properties and current applications of some polysaccharides as biomaterials. *Polym. Int*. 57: 397-430.
42. Sadrnourmohamadi M, Gorczyca B (2015). Removal of dissolved organic carbon (DOC) from high DOC and hardness water by chemical coagulation: relative importance of monomeric, polymeric, and colloidal aluminum species. *Separ. Sci. Technol.* 50:2075-2085.
43. Santos SCR, Boaventura RAR (2008). Adsorption modeling of textile dyes by sepiolite. *Appl. Clay. Sci*. 42:137-145.
44. Singh V, Joung D, Zhai L, Das S, Khondaker S I, Seal S (2011). Graphene based materials: Past, present and future. *Prog. Mater. Sci*. 56:1178-1271.
45. Shelke NB, James R, Laurencin CT, Kumbar SG (2014). Polysaccharide biomaterials for drug delivery and regenerative engineering. *Polym. Adv. Technol*. 25:448-460.
46. Sun X, Sun H, Li H, Peng H (2013). Developing polymer composite materials: Carbon nanotubes or grapheme. *Adv Mater Weinh Ger*. 25:5153-5176.
47. Santos SCR, Boaventura RAR (2008). Adsorption modeling of textile dyes by sepiolite. *Appl. Clay. Sci*. 42:137-145.
48. Su Q, Pang SP, Alijani V, et al (2009). Composites of graphene with large aromatic molecules. *Adv. Mater*. 21:3191-3195.
49. Shi HC, Li WS, Zhong L, et al (2014). Methylene blue adsorption from aqueous solution by magnetic cellulose/graphene oxide composite: equilibrium, kinetics, and thermodynamics. *Ind. Eng. Chem. Res.* 53: 1108-1118.
50. Tao Y, Kong DB, Zhang C, et al (2014). Monolithic carbons with spheroidal and hierarchical pores produced by the linkage of functionalized graphene sheets. *Carbon*. 69:169-177.
51. Tjong SC (2014) Polymer composites with grapheme nano fillers: Electrical properties and applications. *J. Nano. Sci. Nano. Technol*. 14: 1154–1168.
52. Travlou NA, Kyzas GZ, Lazaridis NK, Deliyanni EA (2013). Graphite oxide/chitosan composite for reactive dye removal. *Chem. Eng. J.* 217:256265.
53. Travlou NA, Kyzas GZ, Lazaridis NK, Deliyanni EA (2013). Functionalization of graphite oxide with magnetic chitosan for the preparation of a nanocomposite dye adsorbent. *Langmuir*. 29: 16571668.
54. Yang ST, Chen S, Chang YL, et al (2011). Removal of methylene blue from aqueous solution by graphene oxide. *J. Colloid. Interface. Sci*. 359:24-29.
55. Wang H, Yuan XZ, Wu Y, et al (2013). Adsorption characteristics and behaviors of graphene oxide for Zn(II) removal from aqueous solution. *Appl. Surf. Scim.* 279:432-440.
56. Yao YJ, Xu FF, Chen M, et al (2010). Adsorption behavior of methylene blue on carbon nanotubes. *Bioresource. Technol*. 101:3040-3046.
57. Yongmie H, Zhe W, Jiajia G, and Suying D (2015). Highly efficient adsorption and removal of Chrysoidine Y from aqueous solution by magnetic graphene oxide nanocomposite. *Arabian Journal of Chemistry*. Available online 1 August 2015.
58. Wu ZB, Zhong H, Yuan XZ, et al (2014). Adsorptive removal of methylene blue by rhamnolipid-functionalized graphene oxide from wastewater. *Water. Res*. 67:330344.

59. Zhang X, Rajaraman B R S, Liu H, Ramakrishna S (2014). Graphene's potential in materials science and engineering. *RSC. Adv.* 4: 2898729011.

60. Zhang W, Zhou C, Zhou W, et al (2011). Fast and considerable adsorption of methylene blue dye onto grapheme oxide. *Bull. Environ. Contam. Toxicol*. 87(1):86-90.

How to cite article: Farid Abu Shammala*, Barry Chiswell, Removal of Chrysoidine Y from water by Graphene-based Nanocomposite Derivatives with Magnetic Chitosa Nanocomposite. Int. J. Appl. Pharm. Sci. Res. 4(2):17-33. doi: https://doi.org/10.21477 ijapsr.4.2.2

Source of Support; Nil **Conflict of Interest:** None declared